

# Towards a Droneborne Maritime Lidar for Fisheries Surveys

Michael R. Roddewig<sup>(a)</sup>

<sup>(a)</sup> University of Alaska-Fairbanks Geophysical Institute  
PO Box 757320, Fairbanks, AK 99775, USA  
[mrroddewig@alaska.edu](mailto:mrroddewig@alaska.edu)

**Abstract:** Airborne maritime lidars are an established technique for profiling the underwater environment. However, these lidars required manned aircraft for operation and expensive components. Here, we present the design of a droneborne maritime lidar for salmon surveys. Modeling of the signal-to-noise ratio from a single salmon is considered and we also determine the optimal spot diameter for detection. For the specific water conditions examined, a surface spot diameter of 1-2 m maximizes the detection depth.

## 1. Introduction

Maritime lidars have numerous remote sensing applications, ranging from monitoring of fisheries [1]–[3], profiling of chlorophyll, phytoplankton, and zooplankton [4]–[7], study of internal layers [8], and measurement of water optical properties [9]–[14]. However, maritime lidars that fly on manned aircraft are large and require high-power lasers (with their commensurate eye safety concerns and power draw), expensive detectors, and large receiver telescopes to compensate for the higher minimum safe altitude for a manned aircraft.

Here, we report on the development of a droneborne maritime lidar system. This system is expected to have equivalent penetration performance to larger, existing airborne lidars, due to the dramatically lower altitude a drone can safely operate at (20 m) versus a manned aircraft (300 m). Moving to a droneborne platform will reduce the cost of field experiments and permit new studies. To enable droneborne operation, we are reducing the size, weight, power, and cost (SWaP-C) of previous airborne platforms. Such a reduction has been recently enabled through micropulse lasers and system-on-chip (SoC) miniaturization, where the analog-to-digital converter (ADC), field-programmable gate array (FPGA), and microcontroller are packaged into one integrated circuit.

Our initial interest is in using this lidar system to count salmon at Alaskan salmon hatcheries. Modeling results for the target signal from salmon are presented.

## 2. Design

Fundamentally, a droneborne lidar system takes advantage of the lower flying altitude of a drone to reduce the  $R^4$  loss for a hard target smaller than the beam and thus lower the requirement for a large telescope and powerful laser. Of course, such a reduction in altitude also reduces the swath size of the lidar, but the effect of this limitation is reduced by using a drone platform, which can fly complicated flight patterns for extended endurance times to achieve the same point density as a manned platform.

The lidar under development is a dual-polarization, 1064/532 nm, cross-track scanning, full-wavelength system, targeted to fly on a Spektreworks Cobalt fixed-wing vertical take-off and land (VTOL) platform operated by the Alaska Center for Unmanned Aerial Systems Integration (ACUASI). The Cobalt has an 8 kg payload capacity, 10 hour flight endurance time, and cruise speed of 25 m/s, giving it a range of 900 km. In addition, its VTOL capability enables it to be launched and recovered from ships and remote locations without an airstrip, a significant advantage over manned aircraft.

Of the major components for the lidar, the laser and digitizer presented the most significant challenge for miniaturization. No existing commercial laser met our requirements, so we developed a custom, miniature micropulse 1064/532 nm laser (Figure 1) in collaboration with Quantum Composers, Inc. (Bozeman, Montana, USA). The 1064 nm channel will be used for accurate location of the surface return and the 532 nm channel is the optimal

wavelength for penetration performance in coastal and inland waters where this system is expected to operate. At 532 nm, this laser delivers 34  $\mu\text{J}$ , 1.9 ns pulses at a 100 Hz pulse repetition frequency (PRF). This PRF is low compared to other scanning lidar systems, however, the low flight altitude and slow cruise speed of the Cobalt reduced the PRF requirement which enabled Quantum Composers to achieve a higher pulse energy.

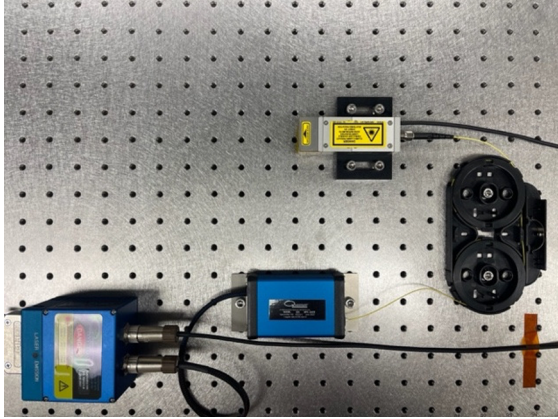


Figure 1. The 1064/532 nm micropulse laser developed with Quantum Composers for the droneborne lidar system.

For the digitizer and lidar controller, we identified the Advanced Micro Devices (AMD) radio frequency system-on-chip (RFSoc) XCZU48DR-1FFVG1517E as an excellent solution. This single-chip solution contains eight 14 bit 5 GSPS analog-to-digital converters (ADCs), four quad-core ARM Cortex-A processors for running software, and programmable logic for generation of the timing and control signals.

Finally, we will use an avalanche photodiode (APD) for the detector, given their compact size and high gain. Initial design was performed with the Thorlabs APD210.

### 3. Modeling

Of significant interest is the selection of appropriate parameters to optimize the detection of salmon. The problem can be described as the detection of a hard target in the presence of significant clutter (i.e. volume scattering from the water and plankton). We wish to determine an appropriate beam area. A large beam area reduces attenuation from the water due to capturing more multiply scattered photons [15], but also reduces the laser power incident on a salmon target and thus the signal

power. A small beam area increases the power density on the salmon target but increases attenuation in the water from photons lost to multiple scattering. Thus, we wish to optimize the beam area for representative water conditions.

To begin, we attack the problem by deriving an appropriate target model for a salmon. Unsurprisingly, quantitative measurements on lidar returns from fish are lacking [16]–[18]. We use the work of Tenningen et al. [18], who compared the reflectivity of live mackerel with a submerged 20% reflective Spectralon target, to derive an approximate lidar cross-section of a salmon by computing the cross-section of a salmon-sized mackerel, yielding a lidar cross-section of  $\sigma = 0.019 \text{ m}^2$  for a  $0.1 \text{ m}^2$  cross-sectional area salmon.

This cross-section, in combination with the performance data of the laser, detector, and other parameters listed below in Table 1, is used to compute the signal-to-noise ratio (SNR) received from a single salmon by the lidar using the hard-target lidar equation. For the noise calculation, system bandwidth was assumed to be the APD210 bandwidth of 1.6 GHz. Noise accounted for detector noise, clutter (volume scattering from water), and background.

**Table 1. Lidar parameters used for modeling**

Symbol	Parameter	Value
$c$	Beam attenuation coefficient	$0.5 \text{ m}^{-1}$
$K_d$	Diffuse attenuation coefficient of downwelling irradiance	$0.15 \text{ m}^{-1}$
$\beta(\pi)$	Volume backscatter of water	$0.0039 \text{ (m-sr)}^{-1}$
$D$	Telescope diameter	50.8 mm
$R_A$	Flight altitude	20 m
$L_B$	Background radiance	$100 \text{ mW m}^{-2} \text{ (nm-sr)}^{-1}$
$B_f$	Interference filter bandwidth	2 nm

To compute the background, we need to consider the receiver field of view (FOV). Our goal is to achieve cross-track scanning of  $\pm 20^\circ$  by mechanically steering the transmit beam and opening up the receive FOV to cover the entire scan area. Thus, the contribution from the

background is a critical consideration. In the flight direction, the receive FOV will be matched to the transmit beam divergence and thus the laser spot size on the water and will be computed for each spot size.

Figure 2 shows an example SNR plot for a single salmon with a 1 m spot size on the water. If we assume a 13 dB SNR requirement for detection, this gives a maximum detection depth of 9.4 m.

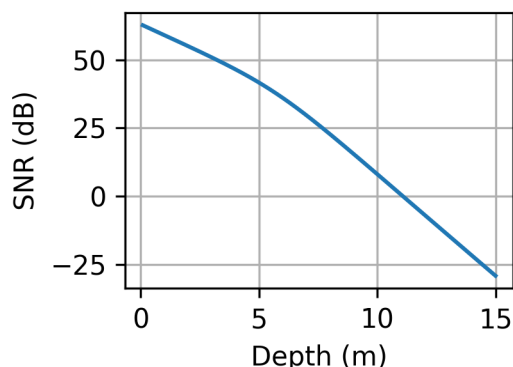


Figure 2. Plot of the SNR for a single salmon with a 1 m spot diameter on the water

Using 13 dB SNR as a rule of thumb for reliable detection, we now want to examine the effect of varying the spot diameter to optimize detection depth. Figure 3 shows the results. Clearly, maximizing the power density on the target by reducing the spot diameter maximizes the penetration depth, even though reducing the spot diameter increases the attenuation in the water. However, a very small spot size has implications for search, requiring numerous spots to effectively cover an area of water. From the plot, we can see that a 1-2 m spot diameter is a happy medium, yielding a maximum

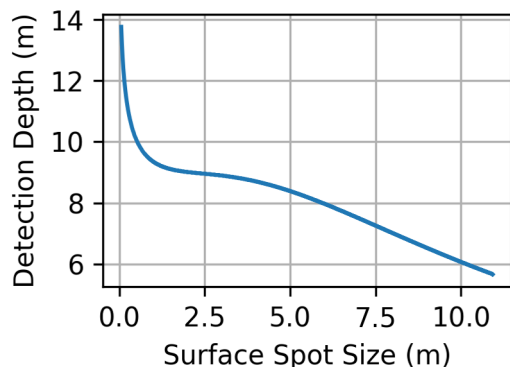


Figure 3. A plot of maximum detection depth of a single salmon versus surface spot diameter.

detection depth of ~9 m for a single salmon. Beyond a 2 m spot diameter, we see that while a larger spot size moves the lidar attenuation into the diffuse regime where attenuation is less, the diminished energy density on the target has the overall consequence of lowering the SNR.

#### 4. Discussion

To further optimize the selection of a spot diameter, we would have to consider the desired coverage of the search volume, which would then consider the laser PRF and drone cruising speed. Eye safety is another critical consideration. Lacking data on the exposure limits for fish, we use the safety thresholds for cetaceans and pinnipeds [19]. To the author's knowledge, no fish have been harmed by lidars operating within these limits. Furthermore, fish that are deeper within the water column receive significantly less exposure than fish near the surface, due to the significant attenuation of light in natural waters.

The optical design of the lidar has not been started. Two challenges will need to be surmounted. First, polarization purity of the transmit laser will need to be maintained over the scan mirror (another reason to limit the spot diameter). Second, we have not determined whether we can achieve the optical throughput for a 40° FOV with the receive telescope. Reduction in the FOV will only improve the SNR results, however, at the cost of scan width.

Finally, an interesting extension of this work would be to analyze the probability of detection and false alarm using the techniques described by Osche in [20]. Previously, Vannoy et al. used machine learning to automate the detection of fish in lidar data [21]. However, to the author's knowledge, no rigorous statistical analysis has yet been undertaken on the automatic detection of fish with lidar.

#### 5. Conclusion

A rigorous analysis of the SNR for detection of salmon with droneborne lidar was presented with an analysis of the maximum detection depth versus surface spot diameter. For the specific water conditions modeled and the case of a single salmon, a spot diameter of 1-2 m was the best compromise between area covered and maximum penetration depth.

## 6. References

- [1] J. H. Churnside *et al.*, “Surveying the distribution and abundance of flying fishes and other epipelagics in the northern Gulf of Mexico using airborne lidar,” *Bulletin of Marine Science*, vol. 93, no. 2, pp. 591–609, 2017, doi: 10.5343/bms.2016.1039.
- [2] E. D. Brown, J. H. Churnside, R. L. Collins, T. Veenstra, J. J. Wilson, and K. Abnett, “Remote sensing of capelin and other biological features in the North Pacific using lidar and video technology,” *ICES Journal of Marine Science*, vol. 59, no. 5, pp. 1120–1130, 2002, doi: 10.1006/jmsc.2002.1282.
- [3] M. R. Roddewig *et al.*, “Airborne lidar detection and mapping of invasive lake trout in Yellowstone Lake,” *Applied Optics*, vol. 57, no. 15, p. 323171, 2018.
- [4] J. H. Churnside, R. D. Marchbanks, and N. Marshall, “Airborne lidar observations of a spring phytoplankton bloom in the western arctic ocean,” *Remote Sensing*, vol. 13, no. 13, Jul. 2021, doi: 10.3390/rs13132512.
- [5] T. S. Moore *et al.*, “Vertical distributions of blooming cyanobacteria populations in a freshwater lake from LIDAR observations,” *Remote Sensing of Environment*, vol. 225, no. September 2018, pp. 347–367, 2019, doi: 10.1016/j.rse.2019.02.025.
- [6] C. A. Hostetler, M. J. Behrenfeld, Y. Hu, J. W. Hair, and J. A. Schullien, “Spaceborne Lidar in the Study of Marine Systems,” *Annual Review of Marine Science*, vol. 10, pp. 121–147, 2018.
- [7] M. J. Behrenfeld, Y. Hu, K. M. Bisson, X. Lu, and T. K. Westberry, “Retrieval of ocean optical and plankton properties with the satellite Cloud-Aerosol Lidar with Orthogonal Polarization (CALIOP) sensor: Background, data processing, and validation status,” *Remote Sensing of Environment*, vol. 281, Nov. 2022, doi: 10.1016/j.rse.2022.113235.
- [8] J. H. Churnside, R. D. Marchbanks, J. H. Lee, J. A. Shaw, A. Weidemann, and P. L. Donaghay, “Airborne lidar detection and characterization of internal waves in a shallow fjord,” *Journal of Applied Remote Sensing*, vol. 6, no. 1, p. 063611, 2012, doi: 10.1117/1.jrs.6.063611.
- [9] J. H. Lee, J. H. Churnside, R. D. Marchbanks, P. L. Donaghay, and J. M. Sullivan, “Oceanographic lidar profiles compared with estimates from in situ optical measurements,” 2013.
- [10] J. H. Churnside, R. D. Marchbanks, C. Lembke, and J. Beckler, “Optical backscattering measured by airborne lidar and underwater glider,” *Remote Sensing*, vol. 9, no. 4, Apr. 2017, doi: 10.3390/rs9040379.
- [11] C. Jamet *et al.*, “Going Beyond Standard Ocean Color Observations: Lidar and Polarimetry,” *Frontiers in Marine Science*, vol. 6, May 2019, doi: 10.3389/fmars.2019.00251.
- [12] H. R. Gordon, “Interpretation of airborne oceanic lidar: effects of multiple scattering,” *Applied Optics*, vol. 21, no. 16, p. 2996, 1982, doi: 10.1364/ao.21.002996.
- [13] M. A. Montes, J. Churnside, Z. Lee, R. Gould, R. Arnone, and A. Weidemann, “Relationships between water attenuation coefficients derived from active and passive remote sensing: a case study from two coastal environments,” 2011.
- [14] M. R. Roddewig, J. H. Churnside, and J. A. Shaw, “Lidar measurements of the diffuse attenuation coefficient in Yellowstone Lake,” *Applied Optics*, vol. 59, no. 10, pp. 3097–3101, 2020, doi: 10.1364/AO.389169.
- [15] J. H. Churnside, “Review of profiling oceanographic lidar,” *Optical Engineering*, vol. 56, no. 7, p. 079802, 2017, doi: 10.1117/1.oe.56.7.079802.
- [16] J. H. Churnside and P. A. McGillivray, “Optical properties of several Pacific fishes,” *Appl. Opt.*, vol. 30, no. 21, p. 2925, Jul. 1991, doi: 10.1364/AO.30.002925.
- [17] J. H. Churnside, J. J. Wilson, and V. V. Tatarskii, “Lidar profiles of fish schools,” *Applied Optics*, vol. 36, no. 24, pp. 6011–6020, 1997.
- [18] E. Tenningen, J. H. Churnside, A. Slotte, and J. J. Wilson, “Lidar target-strength measurements on Northeast Atlantic mackerel (*Scomber scombrus*),” *ICES Journal of Marine Science*, vol. 63, no. 4, pp. 677–682, Jan. 2006, doi: 10.1016/j.icesjms.2005.11.018.
- [19] H. M. Zorn, J. H. Churnside, and C. W. Oliver, “Laser Safety Thresholds for Cetaceans and Pinnipeds,” NOAA, 1998.
- [20] G. R. Osche, *Optical Detection Theory for Laser Applications*. Wiley, 2002.
- [21] T. C. Vannoy *et al.*, “Machine learning-based region of interest detection in airborne lidar fisheries surveys,” *Journal of Applied Remote Sensing*, vol. 15, no. 03, Jul. 2021, doi: 10.1117/1.jrs.15.038503.